

Finite element modeling of compression behavior of extruded polystyrene foam using X-ray tomography

E Sadek and NA Fouad

Journal of Cellular Plastics
49(2) 161–191

© The Author(s) 2013

Reprints and permissions:

sagepub.co.uk/journalsPermissions.nav

DOI: 10.1177/0021955X13477436

cel.sagepub.com



Abstract

Extruded polystyrene rigid foams have attracted a great attention as a superior load-bearing thermal insulation material since their implementation in building construction. One of the most common application areas of this type of thermal insulation material is under raft foundations, where the foam normally undergoes high levels of compression loads. The purpose of this research is to determine how to simulate and optimize the structural response of extruded polystyrene under compression stresses. The optimization has been achieved through investigating the relation between the foam microstructure and the global mechanical properties. The foam was first examined using X-ray tomography imaging technique to acquire some morphological information about the microstructure. The obtained morphological data of extruded polystyrene boards were then utilized to develop microstructure-based finite element models based on the so-called idealized realistic Kelvin cell. The finite element simulation was accomplished with the help of the nanoindentation technology to explore the mechanical properties of the cell wall material. The finite element models were validated by comparisons between the simulated and the experimental results. It has been found that the mechanical properties of the foam in different loading directions can be adequately simulated using the approach of the idealized realistic Kelvin cell. With the help of these models, a parameter study was carried out. This study included the effect of cell size and cell anisotropy on the mechanical response of extruded polystyrene boards under compression stresses. Charts relating between the foam microstructure characteristics and the compression behavior were generated based on the parametric study.

Institute of Building Physics, Leibniz University Hannover, Hannover, Germany

Corresponding author:

E Sadek, Institute of Building Physics, Leibniz University Hannover, Hannover, Germany.

Email: sadek@ifbp.uni-hannover.de

Keywords

Extruded polystyrene boards, compression behavior, X-ray tomography, nanoindentation, microfinite element modeling

Introduction

The requirements to meet constructional heat protection regulations have remarkably increased worldwide in the last few years. These increasing restrictions besides the general trends of low energy and passive homes represent a challenge, which makes thermal insulation materials indispensable.

The application of thermal insulating materials only on structural elements that are exposed to ambient air is not sufficient to meet these requirements. Therefore, construction elements that are adjacent to the soil, such as raft foundation, have to be thermally insulated as well. For this purpose, the full-surface alignment of load-bearing thermal insulation materials under raft foundations is a necessity to minimize the thermal bridges. This application of the insulating material as a load-bearing element induces high compression stress levels in this material. Recently, extruded polystyrene (XPS) rigid boards have emerged as an efficient load-bearing thermal insulation material due to their high load capacity and superior thermal insulation.

To guarantee the structural safety of the buildings constructed with the application of thermal insulation boards under the raft foundation and to avoid any substantial deformations, the structural performance of these boards under compression should be optimized. This optimization could be achieved through establishing the correlation between the mechanical response of these boards and their microstructure configuration.

Literature review

Foams are three-dimensional (3D) cellular materials made from an interconnected network of edges and faces of cells. At the microstructure level, foams could be classified as open-cell and closed-cell foams. If the solid material resides in the cell edge, the cells have open faces and the foam is called open-cell foam. In contrast, the foam is called closed-cell foam when the faces also have solid matter. XPS rigid foams belong to the closed-cell polymer foam type.¹

For a complete understanding of the behavior of the cellular materials or for a better understanding of the main physical phenomena that occur during the use of these materials, the microstructural characterization should be attained and then the relation between this internal structure and the global mechanical properties should be investigated.

A real foam structure, even within a very limited volume of material, is very complicated. It contains cells having many irregularities such as different shapes, distributed cell sizes, cell face curvature, and different solid distributions in the

walls and the ribs or the struts of the cell. In addition, these cells are generally not regularly arranged. However, idealizations make the problem of foam microstructure modeling tractable. The real structure has been usually simulated by many statistically averaged or idealized unit cell shapes packed together. In three-dimensions packing, a great variety of the idealized unit cell shapes is possible.²

For over a century, it was thought that the space filling a cell, which minimizes surface area per unit volume, was the 14-faced Kelvin's tetrakaidecahedron with slightly curved faces.³ Kelvin's cell is broadly applied to this day. Around 100 years after Kelvin et al.⁴ suggested another unit cell having a lower surface area per unit volume than that developed by Kelvin by about 0.3%. This model is too complicated to use and not an attractive option for modeling the foam microstructure. On the contrary, the Kelvin's cell has attracted the attention of many researchers and they have developed models to simulate the mechanical properties of many types of foam materials based on the Kelvin unit cell.⁵⁻¹⁰

Modeling the foam microstructure based on the idealized Kelvin cell ranged from considering that the foam consists of regularly arranged Kelvin cells with a constant wall thickness^{5,6} to a more complicated idealization taking into consideration the irregularity and imperfection in the real foam internal structure. These irregularities include the solid distribution between foam cells and walls^{7,8,10} and the foam cell curvature.^{9,10}

In addition to the solid distribution and the cell face curvature, the disorders in the cell shape include sometimes cell anisotropy or unequal cell dimensions in different directions. The cell shape is governed by the final foam density and the external forces exerted on the cellular structure within the structural phase. In a foam prepared without such external forces, the cell tends to have a high degree of symmetry, i.e. the dimensions of cells in different directions are almost the same. In the presence of the external forces, the cells tend to be elongated or flattened, resulting in anisotropy of cells.¹¹ Almost all manmade foams are anisotropic. However, the structure can still be thought of and simplified as an arrangement of regular cell shapes.²

For example, the cells of some polystyrene rigid foams, especially XPS, can be elongated in the direction perpendicular to the extrusion direction, the rise direction, through manufacturing process. This is attributed to the anisotropic stresses developed by foaming process. Therefore, the compression strength of the XPS boards in the direction perpendicular to the board is higher than that in the other directions.¹² Toward more accurate foam modeling, some researches^{13,14} have modeled the foam microstructure by anisotropic idealized Kelvin cells.

With the purpose of more realistic idealizations in foam modeling, some studies took into account the random arrangement of cells and correspondingly the irregularities in cell shape.¹⁵⁻¹⁸

The high complexity of the foam interior structure and the desire to transfer this complex microstructure geometry directly in numerical simulations without idealizations or even approximations have motivated some researchers to apply some new imaging technologies to build 3D models of the real foam microstructure.

One of the widely known non-destructive techniques to give a 3D picture of the interior structure of cellular solids is the X-ray microcomputer tomography.

The application of X-ray tomography to depict the real structure and shape of the interior of the foam mainly uses two approaches. The first approach is to use X-ray tomography as an imaging process to identify the actual foam architecture, including the strut length and cell size distribution, area and cross-section of the struts, and other morphological characteristics. Afterward, these data are statistically analyzed and utilized to build an idealized foam model based, generally, on the Kelvin's unit cell taking the measured morphological data into considerations.^{15,16,19,20}

For instance, the collected morphological data in the research of Fischer et al.²⁰ have been used to build finite element (FE) meshes using a tessellation of a regular Kelvin unit cell and another tessellation of a modified Kelvin unit cell taking into consideration the various cell sizes. The investigation has shown that the results of the numerical simulations were in a good agreement with those of experimental data. Furthermore, the results for the regular and the modified Kelvin model did not differ much. The difference was not more than 1%–3%.

The second approach of applying X-ray tomography is to develop 3D FE models of the actual geometry of the interior structure of the foam. This is accomplished by examining a small sample from the foam material with X-ray tomography and then developing FE meshes for the 3D solid volume reconstructed from X-ray tomography data without any approximations or idealization.^{21–26} The aim of this approach is to obtain a better agreement between the experimental and the simulated results.

To investigate the properties of the foam parent material or the material of cell walls, in order to be able to accomplish the FE analysis, some researchers have applied the nanoindentation technique.^{24,27}

All literatures surveyed in this research regarding the microstructure of foam materials have revealed that:

- There is a dearth of analyses that have been carried out on the microstructure of XPS rigid boards and its effect on the mechanical behavior of that type of foam.
- In spite of the complexity of the real foam structure, the models based on the regular arrangement of the Kelvin unit cell still represent a promising simple and effective approach to capture the mechanical behavior of cellular materials and the effect of randomness and irregularity of cells on the mechanical response in comparison with the regularly arranged Kelvin cell is marginal.^{15,16,20}
- The limited researches conducted on polystyrene foams^{5,8} tend to model that type of foams as shell elements with constant thickness neglecting the solid distribution between cells struts and walls since the fraction of polymer in the face cells was found to be so high in terms of 0.97 to 0.99.

In the current research, the microstructure configurations of XPS rigid boards were investigated in detail with the help of the X-ray computer tomography imaging

technique. The acquired morphological data were employed to build FE models of the foam microstructure based on the idealized Kelvin cell. The developed models were validated by comparing the simulated results with the experimental ones. The influence of the microstructure configurations on the mechanical response of the foam under compression stresses was studied. Finally, a correlation between the microstructure configurations and the foam compression behavior was established, aiming at optimization of the foam compressive mechanical response.

Foam mechanical behavior characterization

Material

The analyzed foam is one of the commercially available XPS thermal insulation rigid boards with a measured density of 41.2 kg/m^3 and a thickness of 200 mm. The nominal compressive strength of the investigated foam is 300 kN/m^2 . The XPS boards are in the form of a rectangular parallelepiped with length, breadth, and thickness equal to 1200, 600, and 200 mm, respectively.

Compression tests

The response of XPS rigid boards under compression stresses was studied in three main directions. These three directions are parallel to a Cartesian coordinate system whose axes coincide with the three edges of the rectangular parallelepiped XPS rigid board, as shown in Figure 1. The first one, direction (3) in Figure 1, is the conventional loading direction in practice, which is perpendicular to the foam skin and will be called the normal direction. The other two directions, (1) and (2) in Figure 1, are normal to each other and normal to the first direction in the same time. These two directions will be called the transverse and longitudinal directions, respectively.

Nine cube-shaped specimens with edge length equal to the depth of the XPS rigid board were extracted from the XPS boards. Three specimens each of these nine were tested in compression in a different loading direction; three specimens were tested in the normal direction, three in the transversal direction, and three in the longitudinal direction. The compression tests were performed on all specimens in a displacement control mode with a loading rate equal to 10% of the thickness of the tested specimens per minute, complying with DIN EN 826.²⁸

Based on the force–displacement curves obtained by the data acquisition system attached to the testing machine, the stress–strain curves can be plotted, as shown in Figure 2. The stress was calculated as the imposed load divided by the area of the cross-section and the strain as the displacement divided by the initial thickness. The modulus of elasticity can be then determined from the initial slope of the stress–strain curve in the elastic region. It has been noticed that stress–strain curves in all loading directions, as seen in Figure 2, possessed the two distinct regions, namely the linear elastic region arising from elastic bending of cell walls

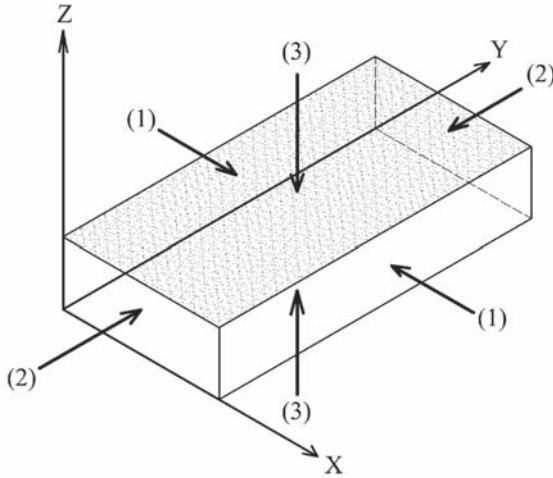


Figure 1. XPS rigid board with the Cartesian coordinate system and compression loading directions.

XPS: extruded polystyrene.

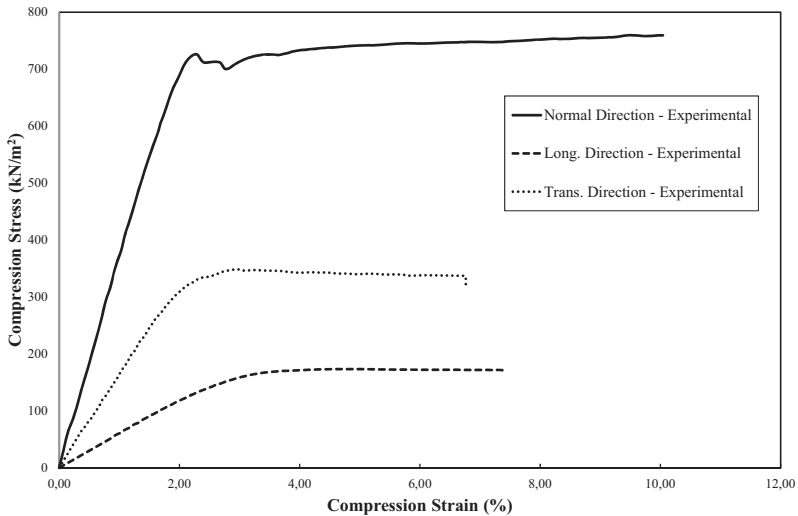


Figure 2. Stress–strain curves under compression in different loading directions.

and followed by the plateau region at higher load levels due to the plastic buckling in cell walls.² As can be seen in Figure 2, the tested XPS rigid boards have direction-dependent mechanical properties under compression stresses. The average compressive strength and modulus of elasticity of the tested samples calculated according to DIN EN 826²⁸ are listed in Table 1.

Table 1. Average mechanical properties under compression in different loading directions.

Mechanical properties	Direction		
	Normal	Transverse	Longitudinal
Young's modulus (kN/m ²)	$E_{33} = 37,010$	$E_{11} = 16,720$	$E_{22} = 5730$
Compressive strength (kN/m ²)	729	347	179

X-ray tomography experimental techniques

Acquisition of X-ray images

The X-ray computer tomography machine Nanotom[®] (GE Sensing and Inspection Technology) was used to perform the X-ray microtomography test. The nanotom[®] machine is equipped with 180kV/15 W ultra high-performance nanofocus tube and precision mechanics for maximum stability. The lowest voxel resolution of this machine reaches 500 nanometer.

The X-ray test was performed on a cubic sample with an edge length of around 5 mm cut out from the XPS board. The experimental implementation of the tomography technique requires three main elements. The first is an X-ray source and the second is a rotation stage on which the sample is fixed. The last main component is the detector. These different parts with the specimens mounted on the rotating stage are shown in Figure 3.

The scanning was started by illuminating the sample with a conical beam of X-ray. The intensity of the X-ray was decreased or attenuated after passing and interacting with the sample and the different intensities of the transmitted X-rays were then recorded on a charge coupled detector camera. This produced two-dimensional images called X-ray projections or back-shadows.²⁹

The sample is then rotated as the back-shadows are recorded at a step size small enough to image the smallest resolvable feature of the structure. Five images were taken at each step to average the data and reduce noise, which is called frame averaging.

The complete analysis was accomplished by a large number of X-ray projections, around 2400, under different viewing angles. Imaging was performed with an effective resolution of 7 μm trying to capture accurately the microstructure details. The acquisition time for each sample was around 3 h.

Image processing

The raw images acquired by X-ray tomography technique or the previously mentioned back-shadows are in the form of grayscale pixels having different gray levels ranging from (0) or black to (255) or white corresponding to 100% X-ray transmission (gas or void phase) and 100% X-ray absorption (solid phase),



Figure 3. The Nanotom[®] machine.

respectively.²⁹ These raw images need to be processed to generate a clear 3D volumetric model of the foam to extract the structural parameters quantifying the foam architecture.

The first step in image processing involved the segmentation process applying the threshold method. In order to ease the segmentation procedure, the grey level images were pre-filtered using a non-linear diffusion filter.³⁰ The result of this smoothing filter is shown in Figure 4(b) and an example of the segmentation result is illustrated in Figure 4(c). This cross-section of the image extracted from segmented volume may be compared with the same cross-section extracted from the original volume without segmentation and filtering shown in Figure 4(a).

Figure 4(a) shows the noise that existed in the raw images arising from the pore absorption of the polystyrene to X-ray. This noise was so high that it was not possible to remove this noise totally by the filtering process, as shown in Figure 4(b). Due to these noisy data, there was usually an overlap in the gray values or the X-ray absorption values of the polymer phase and the void phase. Therefore, the segmentation process resulted often in losing some small details of the foam interior structure, as can be seen in Figure 4(c).

After the segmentation process, the segmented images have been used to generate the 3D surface rendering of the tested specimen, as shown in Figure 5. The noise that appears in the rendered surface has not been removed so as to preserve as much as possible the architecture of the foam.

Quantification analysis

Once the images were segmented, it was possible to first perform a quantitative analysis in order to explore the morphology of the XPS rigid foams. The morphology of any foam could be appropriately characterized mainly by two parameters: the cell size distribution and the wall thickness distribution.

Cell size distribution. The cell size distribution is very easy to obtain when the cells are all perfectly closed. However, the X-ray investigation results revealed that the cells were not completely closed ones but rather interconnected with each other. This can be due to the fact that they are actually interconnected because of the process

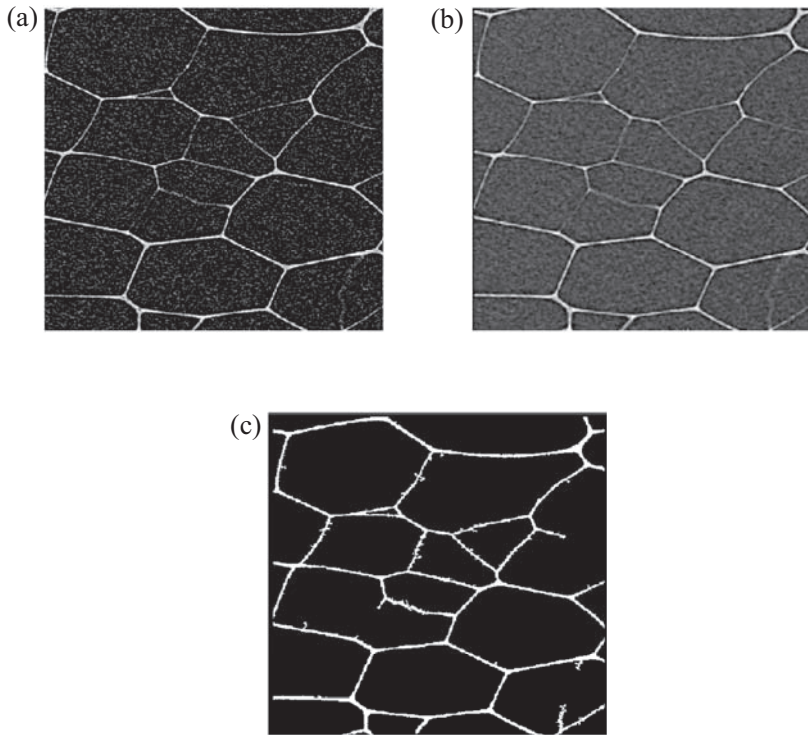


Figure 4. Filtration and segmentation of gray scale images of producer (C). (a) Before Filtering, (b) After Filtering and (c) After Segmentation.

conditions or also that the tomography resolution is not high enough to resolve the thinnest cell walls.

Two possibilities exist to investigate the morphology in the case where the closed cells are interconnected:

- The first possibility is to try to close the cells using morphological operations such as erosion/dilation. When this is done with success, it is possible to extract for each cell every morphological 3D parameter such as volume, surface, aspect ratio, and sphericity.³¹ The cell size distribution can then be easy to obtain since the size is calculated for each cell.
- The second possibility is to use the opening granulometry technique³¹ to retrieve directly the size distribution from the image. This technique can be extended in 3D and it allows measuring the size distribution even if the cells are interconnected. It is worth mentioning that this technique works well when the cells are equiaxed. If the actual cells are not equiaxed, only the smallest dimension of the cell is retrieved.²¹

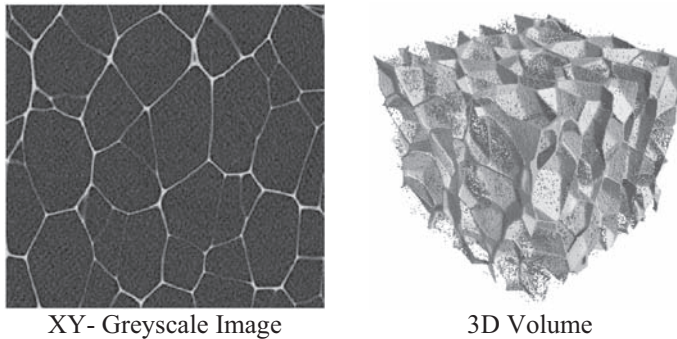


Figure 5. XY images and 2.8 mm^3 3D volume.
3D: three dimensional.

Unfortunately, the two possibilities could not have been applied in this research to extract accurately and automatically the cell size distribution by any specialized computer software. It was not possible to apply the first possibility reasonably to acquire precise data about the cell size due to the inevitable noise in the raw images, which could not be removed, as mentioned before. The optical investigation of the 3D volumes generated by X-ray tomography shown in Figure 5 shows that most of cells are not equiaxed. Therefore, the granulometry technique was expected to yield unrealistic cell sizes.

Due to the inadequacy of the available automatic techniques to collect realistic data to characterizing the foam morphology accurately in the presence of the noise in the images, it was decided that the cell sizes would be measured manually. To do so, around 100 cells were selected randomly from different regions throughout the investigated volume and each of these cells was extracted and its main three dimensions, the length, the width, and the thickness, were then measured, as demonstrated in Figure 6. The rendered surfaces of some extracted cells from the XPS rigid board are illustrated in Figure 7. The length, width, and thickness of the cells were selected parallel to the directions Z, X, and Y, respectively, shown before in Figure 1.

The average of these three dimensions of each cell has been chosen as the parameter that reflects the average size of that cell. The distributions of the three measured dimensions are plotted in Figure 8. According to the dimensions measurements, it was found that the average measured length, width, and thickness of all extracted cells were 1082, 912, and 560 μm , respectively. These results mean that the average cell size of the investigated XPS boards is 851 μm .

One of the most significant results of evaluating the morphology of the XPS board is that all cells were found to be anisotropic. They were always elongated in a certain direction more than the other two directions. The measurements revealed that the biggest dimension, the length of the cell, was primarily the dimension measured perpendicular to the XPS board or perpendicular to the foam skin layer, which exists at the upper and lower surfaces of the XPS board. In addition,

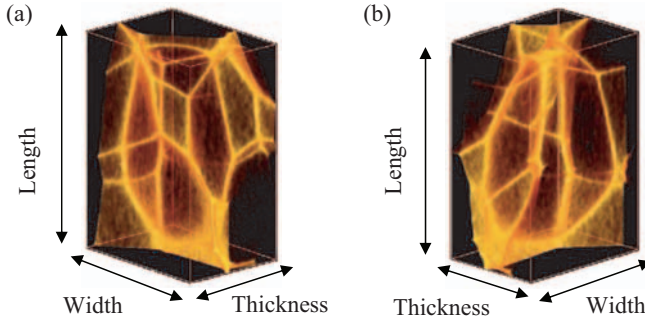


Figure 6. One of the extracted cells and the measured dimensions. (a) 3D View (1) and (b) 3D View (2).

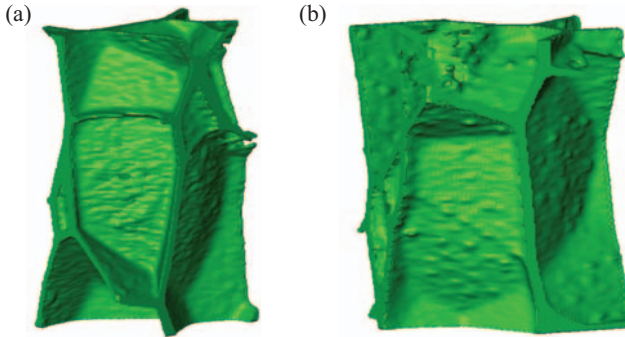


Figure 7. Rendered surface of some extracted cells. (a) Cell (1) and (b) Cell (2).

the smallest cell dimensions, the cell thickness, was found to be in the length direction or the longitudinal direction of the XPS board.

This measured cell anisotropy interprets the experimentally detected anisotropic mechanical behavior of the XPS rigid boards under compression. The measured cell dimensions were found to be in consistent with the detected anisotropic mechanical behavior. The longest dimension of the cells were found in the same direction of the highest compressive strength; the Z-direction in Figure 1. Besides, the shortest dimension of the cells were found in the same direction of the lowest compressive strength: the Y-direction in Figure 1.

Wall thickness distribution. The same manual measuring procedure conducted before to determine the cell size distribution has been performed to provide the wall thickness distribution. Around 100 walls were randomly selected and their thickness was measured. The wall thickness distribution of the investigated specimen is

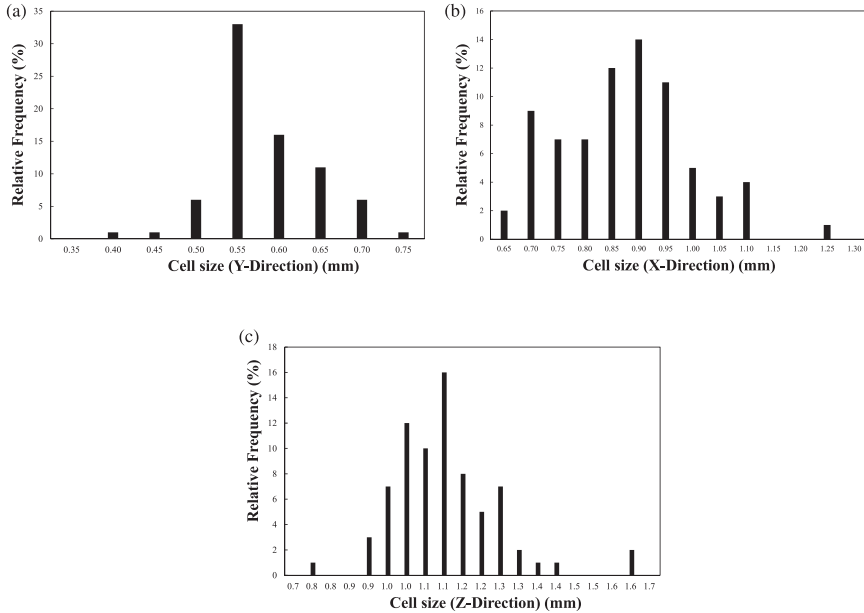


Figure 8. Distributions of the measured cell dimensions. (a) Thickness distribution, (b) Width distribution and (c) Length distribution.

represented graphically in Figure 9. The average wall thickness of the investigated XPS boards was found to be equal to 13.66 μm .

Finite element modeling

Microstructure idealization

The FE modeling in the current research has been carried out based on a simplified interior structure in the form of a uniformly repeated Kelvin cell. This type of simplification, as demonstrated in the literature review, has proved its effectiveness in capturing the realistic mechanical behavior of cellular materials in comparison with other sophisticated approximations.

The original 14-faced Kelvin's tetrakaidecahedron cell is an isotropic cell, i.e. its dimensions in all directions are equal. In addition, the faces of the original Kelvin's cell are slightly curved. In this study, this original cell has been transformed to an anisotropic representative cell with flat surfaces to be used to model the foam structure. This transformation was carried out by modifying the length, width, and thickness of the standard Kelvin cell in accordance with the actual cell average dimensions measured by means of X-ray computer tomography. Moreover,

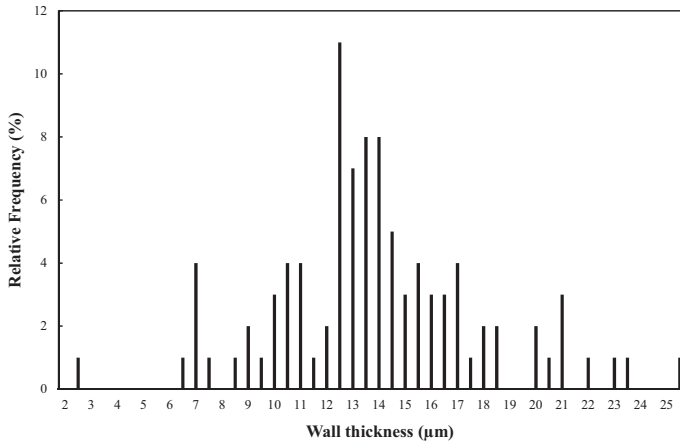


Figure 9. Wall thickness distributions.

the curvature of the cell walls in the original Kelvin cell has been neglected here in the idealized cell.

As has been clarified in the literature review, the closed cell polystyrene foams were efficiently modeled by cells with constant thickness faces neglecting the solid distribution between the walls and struts. The applicability of such simplification on the XPS boards investigated in the current research has been validated by examining the cell walls and struts by X-ray tomography, as shown in Figure 10(a).

X-ray tomography showed that the thickness variation between cell walls and struts in the investigated XPS was marginal compared with other foam types, as shown in Figure 10(b). Therefore, it has been decided to neglect the struts by simplifying the complex microstructure of the XPS foam. As a consequence, the idealized representative cell was taken finally as an anisotropic Kelvin cell composed of flat faces with constant thickness. Afterward, this representative unit cell was regularly arranged beside each other in a body center cubic array to produce the simple regular foam model shown in Figure 11, which was then used to perform the FE analysis. It is worth mentioning that the Cartesian axes shown in Figure 11 coincide with those shown before in Figure 1.

Type of element and boundary conditions

ABAQUS FE code has been employed to perform the FE analysis including pre-processing, solving, and post-processing. There are mainly two types of elements that could be used to obtain the FE meshes of the cellular structure: the continuum elements and the shell elements. Using continuum elements, taking into consideration that the wall thickness is so small compared with the cell size, will lead to using few number of elements across the thickness, which can result in numerical

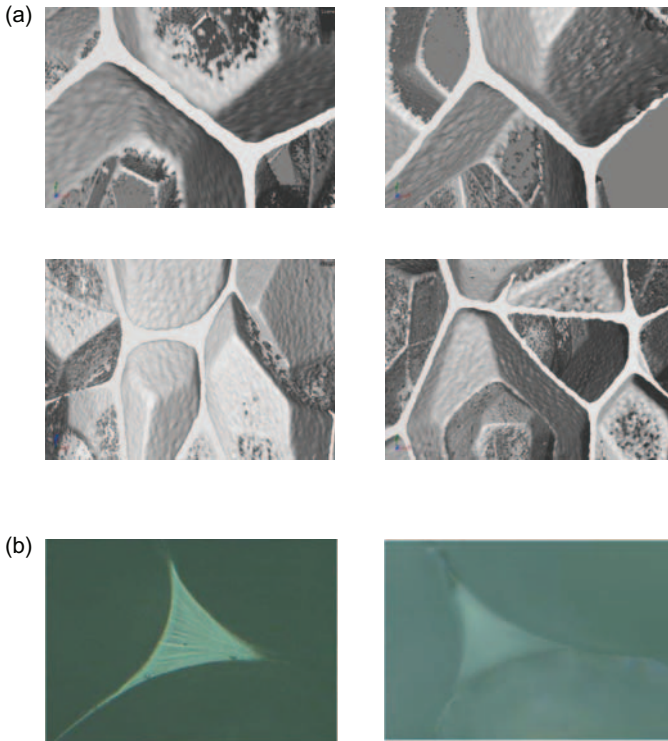


Figure 10. Cell walls and struts of XPS and polyurethane foams. (a) XPS foam and (b) Polyurethane foam.¹³

problems.²¹ Moreover, the research conducted by Caty et al.²⁷ has revealed that continuum FE models should not be applied for closed-cell foams with low relative density. As a consequence, shell elements have been used to mesh the cell faces.

As stated before, the idealized cell consisted only of intersecting flat faces and the mass entrapped at the interfaces of cell walls was found to be small and negligible. Therefore, the whole cell was simply meshed by shell elements only without using any additional element types, such as beam elements, to mesh the intersections of walls. The cell structure was discretized employing the general purpose three-node shell element (S3) from the ABAQUS[®] commercial code.

Boundary conditions must be chosen to properly simulate the experimental conditions. In the performed compression test, one of the clamped sample surfaces rests on the fixed head of the testing machine while the other surface is moved with a constant displacement rate since the testing machine works under displacement control mode. Similarly, a constant vertical deformation was applied to all nodes at the top of the model, while the nodes at the bottom end were not allowed to move in any directions although its rotation degrees of freedom were not constrained.

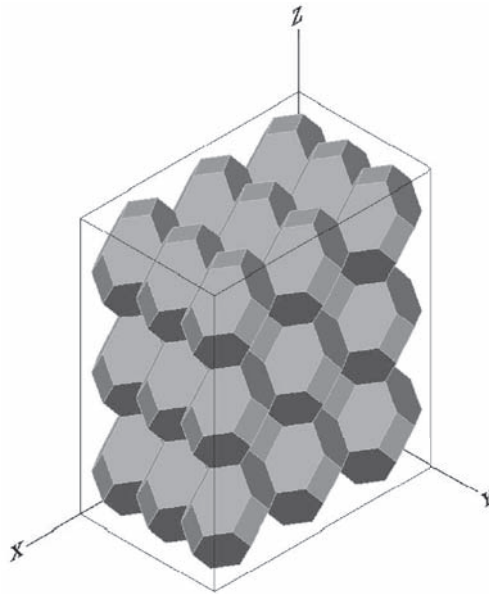


Figure 11. Simplified cellular structure of the investigated XPS boards.
XPS: extruded polystyrene.

Boundary conditions under compression stresses are shown in Figure 12. The boundary condition of the bottom nodes was based on the assumption that the friction generated between the bottom surface of the specimen and the testing machine has prevented the translational degrees of freedom, not the rotational ones.

Parent material property

Through evaluating the grey scale of the monographs representing the densities of the material, it was found that the material is nearly uniform within the cell walls. The parent material was thus assumed to be homogeneous, i.e. the mechanical and physical properties are the same throughout the foam.

The Poisson's ratio of the parent polymer material was taken as 0.35, which is typical for an amorphous polymer at temperatures below the glass transition temperature.²⁴

Since the solid material here is a polymer, the bulk material can be supposed to exhibit a linear elastic-plastic behavior.^{21,24} For the sake of simplicity and since the XPS boards are designed practically so that the applying stresses lies in elastic range of the boards, the solid material are approximated as linear elastic with a constant value of the Young's modulus.

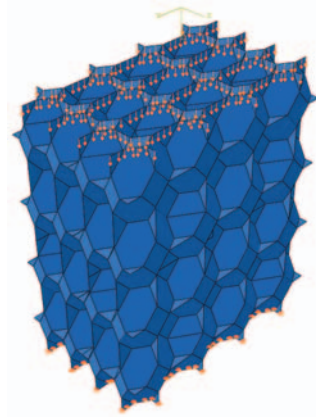


Figure 12. Boundary conditions applied in numerical simulation.

An attempt was made to measure the Young's modulus of cell walls by nanoindentation technique. The nanoindentation experiments were performed by Hysitron TriboIndenter[®] (Hysitron Inc., Minneapolis, MN), using the three-sided pyramidal standard Berkovich indenter tip. The indentation loading segments were designed to include a constant loading rate segment, holding at the maximum load and then unloading. The maximum load was set at 400 μN and both loading and unloading rate has been set to be 40 $\mu\text{N}/\text{sec}$. Guided by the research of Brisco et al.,³² the maximum indentation load was held for around 10 s in order to minimize the creep-like behavior on the unloading curve.

Practically and in the frame of the current research, carrying out the nanoindentation technique directly on the cell walls with their very small thicknesses was inconvenient and has yielded redundant and unrealistic values of the elastic modulus. The discrepancy of the elastic modulus results could have emerged from the variation of the stiffness of the wall itself from one testing point to the other, depending on the relative orientation between the indenter and the wall. Second, the very small thickness of walls in addition to the air voids between these walls has contributed to the unrealistic low values of the Young's modulus yielded from nanoindentation test. More details about the nanoindentation challenges in polymers and foams and its solutions could be found in other studies^{24,33,34}

Therefore, it was decided that a small sample extracted from the XPS boards would be heated to 200°C and then this sample was manually pressed with the purpose to transform the foam sample to a solid polymer one. Nanoindentation test was then performed on three different positions in the polymer sample. The average load versus displacement curve during nanoindentation is illustrated in Figure 13.

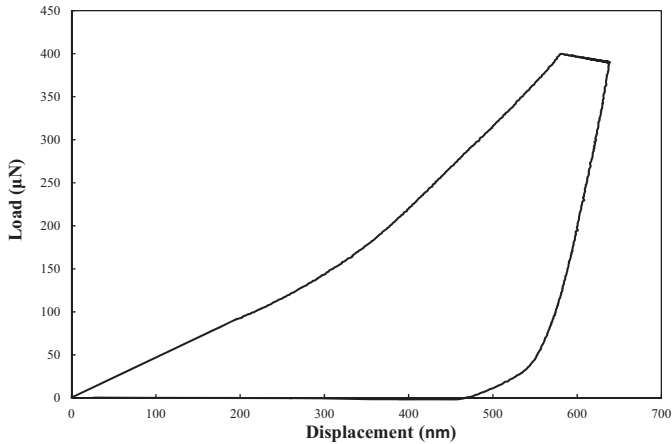


Figure 13. Load–displacement curve in nanoindentation test.

Applying the Oliver and Pharr method³⁵ on the unloading segment in the load–displacement curve shown in Figure 13 yielded a value of the elastic modulus of the tested specimen equal to 1410 MPa. To check the soundness of the nanoindentation test result, the results of the Young’s modulus were compared with any documented values of the elastic modulus of the polystyrene. Matonis³⁶ suggested a value of 1380 MPa and 1050 kg/m^3 for the Young’s modulus and density, respectively, of the rigid polystyrene. Approximately same values were stated by Chan and Nakamura³⁷ for the solid XPS. Therefore, it could be concluded that the nanoindentation test result does not deviate significantly from the values that existed in the reference texts. The elastic modulus value that resulted from nanoindentation was therefore applied in the FE analysis.

It is worth mentioning that the gas pressure inside the foam closed cells was ignored in the FEM by the current research. This is based on the assumption that by small deformations, like the deformations considered in the numerical modeling in this study, which was not more than 1%, the air pressure could not have a significant effect. The air pressure should be taken into consideration by investigating the post-buckling behavior of foam or the post-yielding hardening.⁸ Second, under the low loading rate in the current research, unlike the high loading rates such as dynamic tests, the gas pressure inside cells is not expected to play a remarkable role in the mechanical properties of the tested foam.

Moreover, it is well known that foam cell walls undergo biaxial extension during foam expansion, which could modify the modulus of the polymer and its yield stress. This effect was ignored in the current research based on the conclusion of Mills and Zhu.⁸ They have found out that the Young’s modulus of the biaxially oriented polystyrene film is the same for unoriented bulk polystyrene.

Model size

The size of the modeled microstructure should be so selected to yield a consistent mechanical behavior. To find the appropriate model size, stepwise increase of the volume of the model was considered. The smallest of these models was with the size of two cells in each of the three orthogonal coordinates and the biggest was with the size of five cells in each direction, as shown in Figure 14. The maximum model size is limited by the available computational power to mesh and to compute the model. Therefore, it was not possible to consider models with a size bigger than five cells in each direction.

It has to be mentioned here that the FE analysis using the implicit solution technique in Abaqus became unstable after the beginning of cell wall buckling. Therefore, it was not possible to complete the analysis in the post-buckling region. An alternative solution to capture the whole structural response was to perform the post-buckling analysis applying the explicit scheme rather than the implicit one, i.e. treating the buckling response dynamically.⁵ The post-buckling analysis lies outside the main aspect of the this research.

The stresses for the foam models were computed by dividing the reaction force experienced by the movable nodes by the respective tributary area of the model perpendicular to the loading direction. The engineering compression strain was obtained by dividing the vertical displacement of the movable nodes by the height of the model.

The stress–strain curves shown in Figure 15 refer to the marginal effect the model size has on the elastic response of the foam model under compression stresses where all models had approximately the same elastic modulus. The model size effect is expected to be detectable in the inelastic zone or after the onset of the plateau due to the different buckling modes of different models. This is consistent with the conclusion revealed by the investigation of Jang et al.¹⁶ Since the post-buckling behavior lies beyond the scope of the current research, the two cells based model was considered in the further analysis to save computational time.

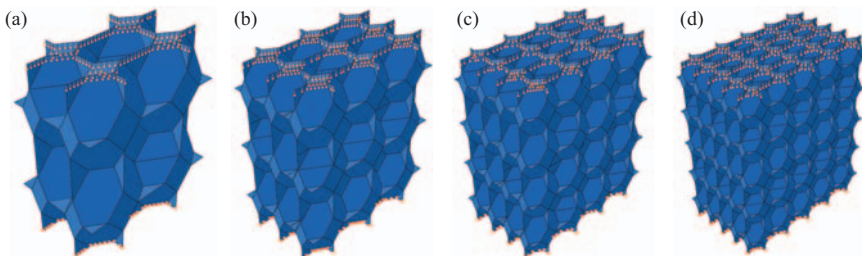


Figure 14. Different sizes of models in simulation of compression test. (a) Two-cells model, (b) Three-cells model, (c) Four-cells model and (d) Five-cells model.

Model convergence mesh size dependency

To be able to perform the mesh sensitivity analysis, the mesh density (MD) has been utilized. The MD is defined in this study as the number of elements in each unit cell of the model. The MD can be calculated as the total number of elements of the model divided by the number of cells included in that model. The advantage of the MD concept is its applicability on different foams with different cell sizes independent from the absolute size of FE used in model discretization. Therefore, the outcome of the mesh sensitivity analysis performed in this section could be taken as a guide when modeling other foams with different cell size.

Six calculations were performed on the same model, as shown in Figure 14(a), using the same boundary conditions and the same material properties. Each calculation was carried out using different mesh size. Table 2 summarizes the characteristics of these six models. The MD was calculated considering that the number of cells in the compression model was taken equal to four cells.

In order to study the convergence of the calculation, it has been focused on one of the outputs of the simulation, namely the Young's modulus (E). Using this output, the normalized difference of the elastic modulus value of each model has been calculated relative to that of the model with the finest mesh (E_*). The normalized difference of Young's modulus (ΔE_i) was calculated as $\Delta E_i = (E_i - E_*)/E_*$, where (E_i) is the elastic modulus of each model. These normalized differences are reported in Table 2 and the change in the resulting Young's modulus with the used MD is plotted in Figure 16.

Table 2 and Figure 16 show that the calculations converge to approximately a constant behavior when the MD is more than around 13,000 elements per cell

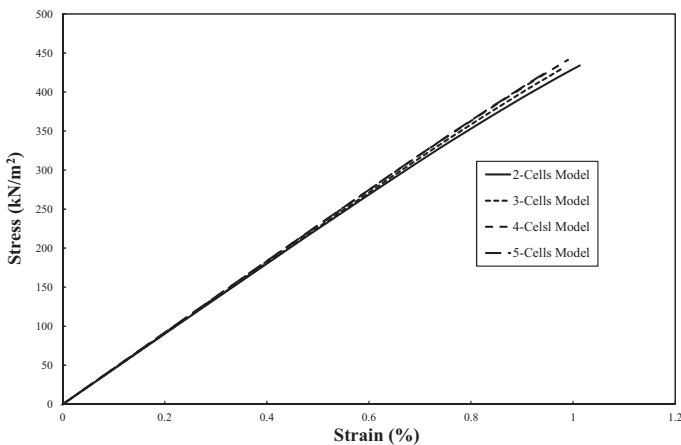
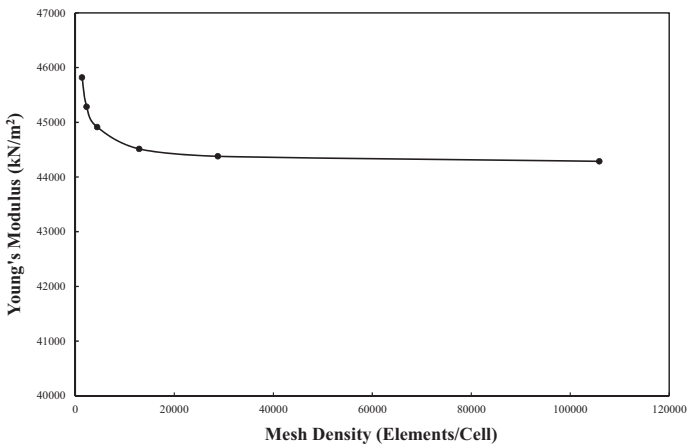


Figure 15. Compression stress–strain curves of different sizes of model.

Table 2. Effect of mesh resolution on the Young's Modulus.

Model reference	Number of elements	MD (elements/cell)	Young's Modulus relative difference (%)
Model 1	423,514	105878	0.00
Model 2	115,116	28779	0.21
Model 3	51,534	12883	0.51
Model 4	17,634	4408	1.41
Model 5	9070	2267	2.25
Model 6	5370	1342	3.46

MD: mesh density.

**Figure 16.** Effect of mesh density on compression Young's modulus.

corresponding to model 3. The computation time is another factor that should be taken into consideration. It was found that the computation time of model 3 is around three times more than that of model 4, while the error made on (E_*) using model 4 was less than 2%. As a consequence, model 4 appears to be an efficient trade-off between model resolution and time consumption by compression test simulation.

Model validation

To ensure the accuracy and the validity of the current microstructure-based FE models, the numerical simulation results were compared with the experimental ones.

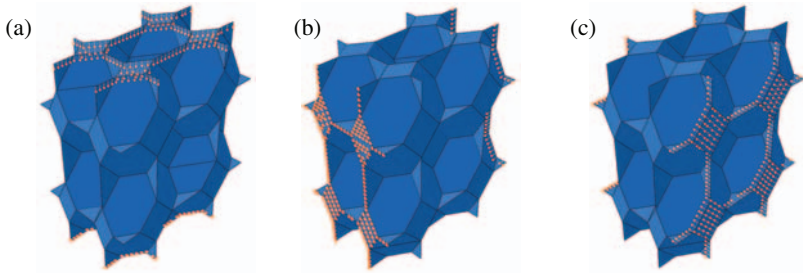


Figure 17. Numerical simulation of compression test in different loading directions. (a) Normal direction, (b) Transverse direction and (c) Longitudinal direction.

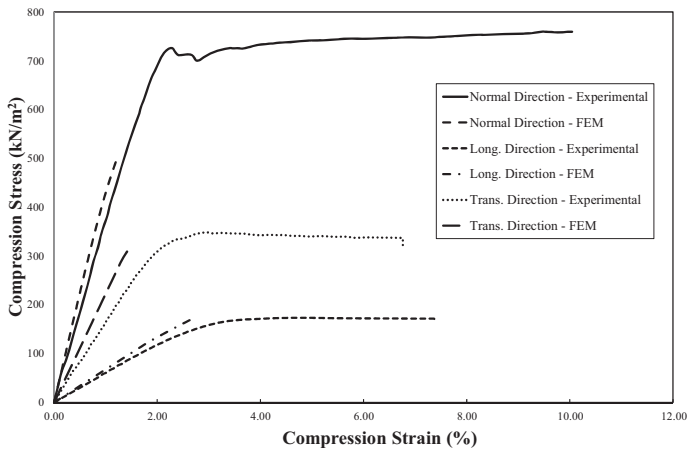


Figure 18. Comparison between simulated and experimental response under compression stresses.

The established FEM model for compression test, the two-cell model shown in Figure 14, was used to perform the numerical simulation to predict the mechanical properties, namely the elastic modulus, under compression stresses in the three orthogonal loading directions illustrated in Figure 1: the normal, transverse, and the longitudinal directions. The three FEM models in the three loading directions with the applied displacements and their boundary conditions are shown in Figure 17. Measured and calculated compression stress–strain curves are plotted against each other in Figure 18. The simulated and the measured Young’s modulus and the difference between them are listed in Table 3.

The comparison between the simulated and the experimentally measured compression elastic modulus has revealed that FE simulation yielded an overestimated Young’s modulus in all loading directions. The overestimation was between 15% and 35% more than the measured modulus, as listed in Table 3. This overestimation can be attributed mainly to the idealization process applied to develop the

Table 3. Comparison of experimental and simulated values of compressive modulus.

Loading direction	Compressive modulus (kN/m ²)		Relative difference in Young's modulus (%)
	Simulated	Experimental	
Normal	42,800	37,008	15.65
Longitudinal	6770	5734	18.07
Transverse	22,270	16,719	33.20

foam microstructure, i.e. the imperfections that already existed in the foam cells were not taken into consideration in FE analysis. One of the significant imperfections that was not considered in the idealization was the cell wall curvature. The different degree of cell wall curvature in normal, transversal, and longitudinal directions might explain the variant bias between the simulated and experimental results shown in Table 3.

Despite the difference noticed between the simulated and the measured elastic modulus under compression stresses, it can be stated that the microstructure-based FE analysis employing the regular anisotropic Kelvin's Cell is able to reproduce the short-term mechanical response of XPS boards under compression stresses in all investigated loading directions with an acceptable accuracy level, as can be seen in Figure 18.

It has to be mentioned here that the FE analysis using the implicit solution technique in Abaqus became unstable after the beginning of cell wall buckling. Therefore, it was not possible to complete the analysis in the post-buckling region. An alternative solution to capture the whole structural response was to perform the post-buckling analysis applying the explicit scheme rather than the implicit one, i.e. treating the buckling response dynamically³⁸ or applying other solution methods, instead of the Newton's method, to solve the nonlinear FE try and error equations such as Riks method.³⁹

The post-buckling analysis lies outside the main aspect of the current research since, as mentioned before, the load levels in the creep tests lie within the elastic range of the mechanical response of the XPS rigid boards. For this reason, the focus in this research was on the elastic domain only.

Parametric study

The major advantage of microstructure-based modeling of foams, as referred to before, is the ability to correlate between the microstructure characteristics of these materials and their physical and mechanical properties aiming to optimizing these properties. For this purpose, the FE model developed to simulate the compressive response of XPS boards was employed for conducting a series of parametric studies. The objective was to investigate the influence of the variation of cell size and

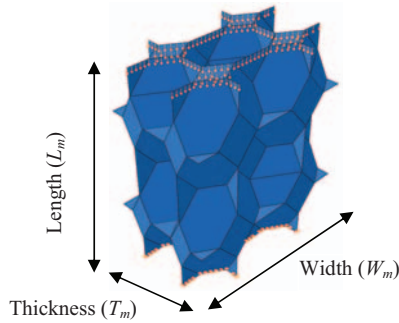


Figure 19. Model dimensions used to calculate the model volume.

cell anisotropy on the mechanical performance of the XPS rigid boards under compression stresses.

Variation of cell size

The model shown before in Figure 14(a) was employed to investigate the impact of the cell size on the mechanical behavior of XPS boards. The cell wall thickness has to be changed with the change of the cell size so that the foam relative density ($R.D.$) remains constant to eliminate the impact the relative density has on the foam properties. The foam relative density was calculated according to the relation:

$$R.D. = \frac{A_w \Delta t_w}{V_m}, \quad (1)$$

where (A_w) is the surface area of the cell walls in the model, calculated with the help of Abaqus, (t_w) is the cell wall thickness, and (V_m) is the model volume calculated as ($V_m = L_m \times T_m \times W_m$), as illustrated in Figure 19. The model volume varied with changing the cell size and the wall thickness was altered in each case depending on the area of cell faces to yield the same relative density for all considered cell sizes.

The original average cell size, obtained from the X-ray tomography measurement, was taken as the reference cell size (100%). The cells in the FE model have then been resized to represent 50%, 75%, and 125% of the reference cell size. The simulated compression stress–strain curves of the models resulting from these different cells are shown in Figure 20. The numerical results have revealed that the cell size has no effect on the foam mechanical response as long as the foam relative density remains unchanged.

Variation of cell anisotropy

The unequal dimensions of the cell, L, D, and H, measured in the direction of the three principal orthogonal axes, as shown in Figure 21, is referred to in this study

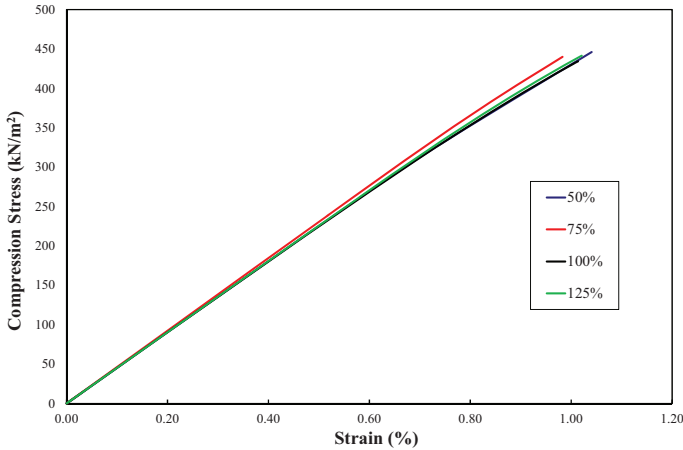


Figure 20. Simulated compression stress–strain curves of models with different cell sizes (the density was held constant by changing the wall thickness as the cell size is changed).

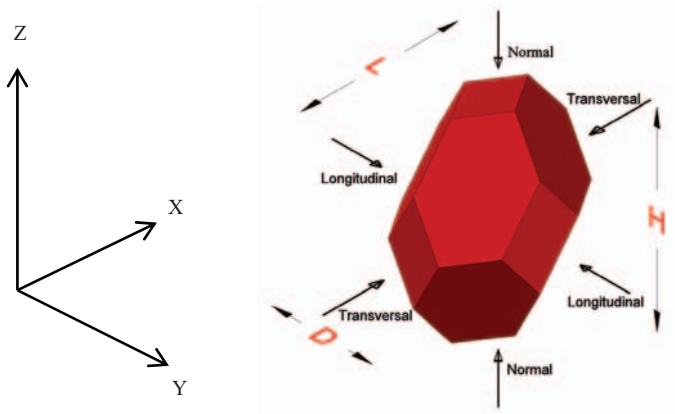


Figure 21. Three-dimensional schematic illustration of cell anisotropy.

as cell anisotropy. The three Cartesian axes *X*, *Y*, and *Z*, shown in Figure 21 have the same orientation relative to the XPS board, shown previously in Figure 1. This means that the axes *X*, *Y*, and *Z* shown in Figure 21 correspond to the breadth, length, and thickness of the XPS board, respectively.

Considering that the cell size itself has no impact on foam mechanical behavior, it was decided that the influence of the cell dimensions relative to each other would be investigated, not the absolute value of these dimensions. Therefore, it was more useful to subsequently use the dimensions shown in Figure 21 to refer to the cell relative dimensions instead of the absolute cell dimensions.

Aiming to cover most of the possible combinations of the cell relative dimensions (L, H, and D), the relative cell height (H) was held constant and equal to unity, whereas the relative cell dimension (D) has been changed from 0.40 to 1.00. At each value of (D), the relative cell dimension (L) varied between 0.40 and 1.00 as well. This means that totally 49 different combinations of the relative cell dimensions have been investigated, as shown in Table 4.

To calculate the corresponding absolute cell dimensions to be used to build the FE models, the height of the average cell (1.082 mm), which was measured before by X-ray tomography, has been taken as the reference dimension and all other dimensions were calculated proportional to that one. As a clarification, some of the analyzed cells with different relative dimensions and the corresponding FE models are shown in Figure 22. As mentioned before, to avoid the effect of the foam relative density that arises from changing the cell dimensions, the wall thickness has been changed in each dimension combination applying Equation (1). The considered relative dimension combinations and their corresponding absolute cell dimensions and wall thicknesses are shown in Table 4.

With the help of the developed FE models, the effect of the cell anisotropy on the elastic moduli in the three orthogonal directions, shown previously in Figure 1, was investigated. For this purpose, three FE models were developed for each cell relative dimensions combination, similar to those shown in Figure 17, to be used to estimate the three elastic moduli. The relation between the cell relative dimensions and the three mechanical properties, normal, longitudinal, and transversal compression elastic modulus, was plotted (Figures 23 and 24).

The soundness of these figures has been assessed by employing them to estimate the foam mechanical properties. The measured cell dimensions were used to calculate the cell dimensions (L and D) relative to the cell height (H). The calculated ratios were equal to $L/H = 0.842$ and $D/H = 0.518$. These relative dimensions were then used to extract the three foam mechanical properties stated previously.

The values extracted from Figures 23 and 24 are appropriately comparable to the corresponding simulated ones listed previously in Table 1. This means that these curves could be used to assess these compression properties of the investigated XPS boards after the acquisition of the cell relative dimensions with the help of the X-ray tomography technique.

The investigation of the influence of the cell relative dimensions on the foam compression behavior has revealed that while decreasing the relative dimensions (L/H) enhances the elastic modulus in the normal direction, decreasing this value to unacceptable levels has its negative influence on the elastic modulus in the transversal direction, as shown in Figure 23. In addition, the analysis results showed that decreasing the value (D/H) affected positively the elastic modulus of elasticity in both normal and transversal directions (Figure 23), whereas this reduction had a negative impact on the elastic modulus in the longitudinal direction (Figure 24).

Therefore, Figures 23 and 24 are very helpful to design the microstructure configuration of the XPS boards accommodating with the surrounding loading

Table 4. The different combinations of cell relative dimensions and the corresponding absolute dimensions and wall thicknesses analyzed.

Dimensions ratio			Absolute dimensions (mm)			Area of faces (mm ²)	Wall thickness (μm)
H	D	L	H	D	L		
1.00	0.40	0.40	1.082	0.433	0.433	11.07	9.45
		0.50			0.541	12.64	10.34
		0.60			0.649	14.30	10.97
		0.70			0.757	16.02	11.42
		0.80			0.866	17.80	11.75
		0.90			0.974	19.59	12.01
		1.00			1.082	21.40	12.22
1.00	0.50	0.40	1.082	0.541	0.433	12.64	10.34
		0.50			0.541	14.19	11.52
		0.60			0.649	15.84	12.38
		0.70			0.757	17.57	13.02
		0.80			0.866	19.37	13.50
		0.90			0.974	21.19	13.88
		1.00			1.082	23.05	14.18
1.00	0.60	0.40	1.082	0.649	0.433	14.30	10.97
		0.50			0.541	15.84	12.38
		0.60			0.649	17.50	13.45
		0.70			0.757	19.25	14.26
		0.80			0.866	21.08	14.88
		0.90			0.974	22.95	15.38
		1.00			1.082	24.85	15.78
1.00	0.70	0.40	1.082	0.757	0.433	16.02	11.42
		0.50			0.541	17.57	13.02
		0.60			0.649	19.25	14.26
		0.70			0.757	21.03	15.23
		0.80			0.866	22.90	15.98
		0.90			0.974	24.81	16.60
		1.00			1.082	26.78	17.09
1.00	0.80	0.40	1.082	0.866	0.433	17.80	11.75
		0.50			0.541	19.37	13.50
		0.60			0.649	21.08	14.88
		0.70			0.757	22.90	15.98
		0.80			0.866	24.82	16.85
		0.90			0.974	26.79	17.57
		1.00			1.082	28.82	18.14

(continued)

Table 4. Continued

Dimensions ratio			Absolute dimensions (mm)			Area of faces (mm ²)	Wall thickness (μm)
H	D	L	H	D	L		
1.00	0.90	0.40	1.082	0.974	0.433	19.59	12.01
		0.50			0.541	21.19	13.88
		0.60			0.649	22.95	15.38
		0.70			0.757	24.81	16.60
		0.80			0.866	26.79	17.57
		0.90			0.974	28.83	18.36
		1.00			1.082	30.93	19.02
1.00	1.00	0.40	1.082	1.082	0.433	21.40	12.22
		0.50			0.541	23.05	14.18
		0.60			0.649	24.85	15.78
		0.70			0.757	26.78	17.09
		0.80			0.866	28.82	18.14
		0.90			0.974	30.93	19.02
		1.00			1.082	33.10	19.75

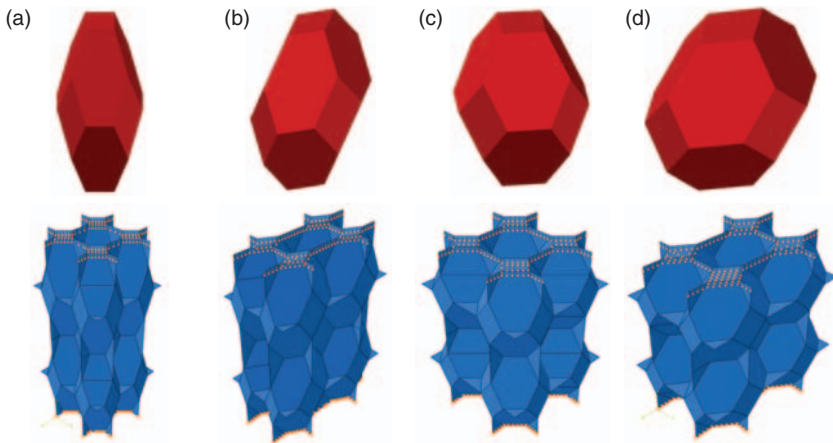


Figure 22. Schematic illustration of cells and the corresponding FE models with different combinations of cell relative dimensions. (a) $H = 1.0$, $D = 0.40$, $L = 0.40$, (b) $H = 1.0$, $D = 0.40$, $L = 0.70$, (c) $H = 1.0$, $D = 0.70$, $L = 0.70$ and (d) $H = 1.0$, $D = 0.70$, $L = 1.0$
FE: finite element.

conditions. Moreover, these curves can be used to maximize the compressive behavior in the normal direction without notable reduction in the compressive response in the other directions, which is of great importance knowing that the ratio of the compressive strength in the different directions of the produced XPS

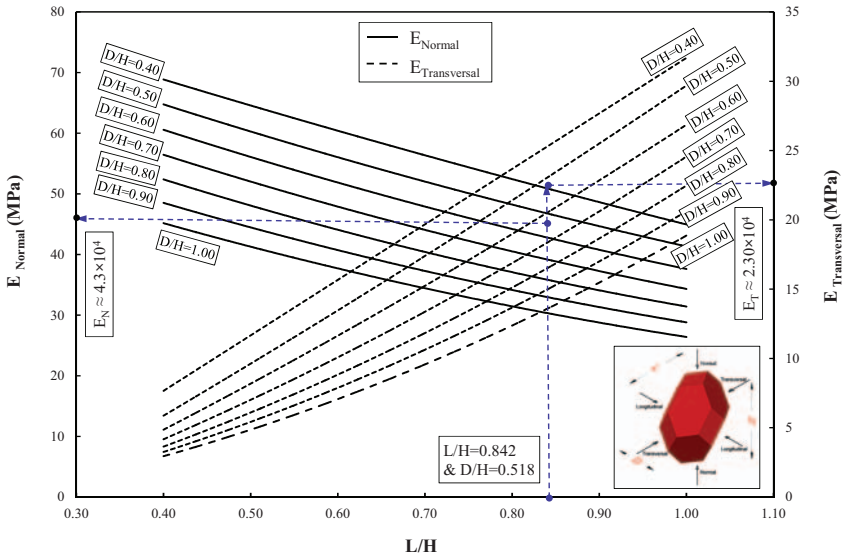


Figure 23. Effect of cell anisotropy on elastic modulus in normal and transversal directions.

boards must comply with some specified limits for the produced boards to be approved as an acceptable industrial product.

Summary and conclusions

The primary goals of this study were to simulate the compression behavior of XPS rigid foam based on the foam microstructure applying the X-ray microcomputer tomography and to optimize the foam mechanical response under compression stresses. The optimization was based on investigating the impact of the cell structure configuration on the foam global compressive behavior using microstructure-based FE models.

The following conclusions were drawn from the experimental and analytical work carried out in this study:

- XPS rigid boards have orthotropic mechanical behavior under compression stresses, i.e. the mechanical properties are direction dependent. The highest compressive strength was in the direction perpendicular to the foam skin layer. The cell structure as captured by X-ray tomography agrees with this conclusion. The cells were found to be anisotropic and the biggest dimension was always in the direction normal to the foam skin, which explains the high compressive strength and Young’s modulus detected in this direction.
- The solid distribution between the cell walls and the struts in the investigated XPS rigid boards could be neglected, i.e. these types of boards can be modeled by cells with constant thickness faces.

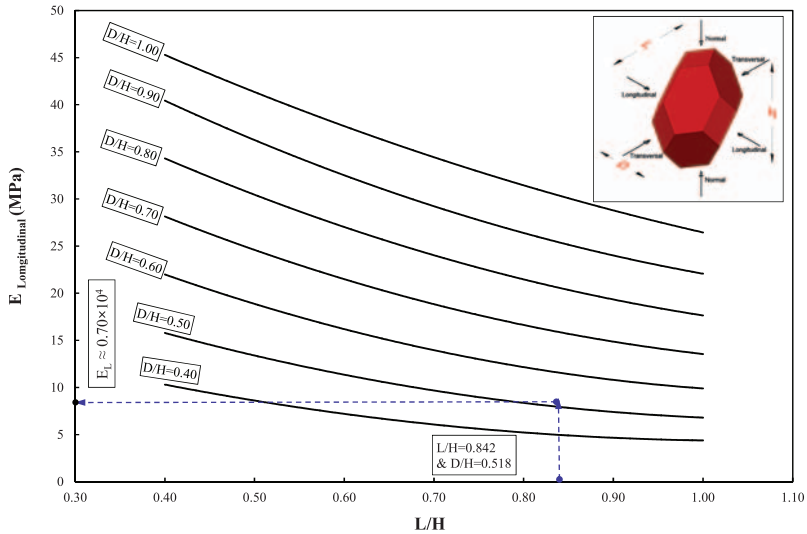


Figure 24. Effect of cell anisotropy on elastic modulus in the longitudinal direction.

- Idealization of the complicated XPS foam microstructure morphology based on the standard Kelvin cell taking into consideration the anisotropy of the realistic cells represents a promising approach to develop microstructure-based FE models simulating accurately the foam mechanical behavior.
- The microstructure cell size has no impact on the compression mechanical properties of the XPS rigid boards as long as the density of these boards remains constant. On the contrary, the degree of cell anisotropy has a crucial influence.
- By optimizing the foam compressive behavior in the normal direction, in which the XPS boards are practically highly loaded, the corresponding reduction in the foam mechanical behavior in the other directions has to be taken into account.

Funding

This research was supported and funded through the institute of Building Physics, Leibniz University Hannover, Germany.

References

1. Placido E, Arduini-Schuster MC and Kuhn J. Thermal properties predictive model for insulating foams. *Infrared Phys Technol* 2005; 46: 219–231.
2. Gibson LJ and Ashby MF. *Cellular solids*, 2nd Edition. Cambridge, UK: Cambridge University Press, 1999.
3. Thomson W and Kelvin L. The division of space with minimum partitional area. *Philos Mag* 1887; 24: 503.
4. Weaire D and Phelan R. Counterexample to Kelvin's conjecture on minimal surfaces. *Phil Mag Lett* 1994; 69: 107–110.

5. Nammi SK, Myler P and Edwards G. Element analysis of closed-cell aluminum foam under quasi-static loading. *Mat Des* 2010; 31: 712–722.
6. Mills NJ, Stämpfli R, Marone F, et al. Finite element micromechanics model of impact compression of closed-cell polymer foams. *Int J Solids Struct* 2009; 46: 677–697.
7. Simone AE and Gibson LJ. Effects of solid distribution on the stiffness and strength of metallic foams. *Acta Mater* 1997; 46: 2139–2150.
8. Mills NJ and Zhu HX. The high strain compression of closed-cell polymer foams. *J Mech Phys Solids* 1999; 47: 669–695.
9. Simone AE and Gibson LJ. The effects of cell face curvature and corrugations on the stiffness and strength of metallic foams. *Acta Mater* 1998; 46: 3929–3935.
10. Giorgi M, De, Carofalo A, Dattoma V, et al. Aluminum foams structural modelling. *Comp Struct* 2010; 88: 25–35.
11. Suh KW. Polystyrene and structural foam. In: Klempner D, Frisch KC (eds) *Handbook of polymeric foams and foam technology*. München, Wien: Hanser, 1991.
12. Waßner KH. Anwendungstechnische Eigenschaften von PS-Hartschaum. In: Gausepohl H, Geller R (eds) *Kunststoff handbuch 4: polystyrol*. München, Germany: Hanser, 1996.
13. Ridha M and Shim VPW. Microstructure and tensile mechanical properties of anisotropic rigid polyurethane foam. *Exp Mech* 2008; 48: 763–776.
14. Gong L, Kyriakides S and Jang W.-Y. Compressive response of open-cell foams. Part I: morphology and elastic properties. *Int J Solids Struct* 2005; 42: 1355–1379.
15. Jang WY, Kraynik AM and Kyriakides S. On the microstructure of open-cell foams and its effect on elastic properties. *Int J Solids Struct* 2008; 45: 1845–1875.
16. Jang W-Y, Kyriakides S and Kraynik AM. On the compressive strength of open-cell metal foams with Kelvin and random cell structures. *Int J Solids Struct* 2010; 47: 2872–2883.
17. Roberts AP and Garboczi EJ. Elastic moduli of model random three-dimensional closed-cell cellular solids. *Acta Mater* 2001; 49: 189–197.
18. Schulmeister V, Van der Burg MWD, Van der Giessen E, et al. A numerical study of large deformations of low-density elastomeric open-cell foams. *Mech Materials* 1998; 30: 125–140.
19. Montminy MD, Tannenbaum AR and Macosko CW. The 3D structure of real polymer foams. *J Colloid Interface Sci* 2004; 280: 202–211.
20. Fischer F, Lim GT, Handge UA, et al. Numerical simulation of mechanical properties of cellular materials using computed tomography analysis. *J Cellular Plast* 2009; 45: 441–460.
21. Maire E, Fazekas A, Salvo L, et al. X-Ray tomography applied to the characterization of cellular materials: related finite element modeling problems. *Compos Sci Technol* 2003; 63: 2431–2443.
22. Youssef S, Maire E and Gaertner R. Finite element modelling of the actual structure of cellular materials determined by X-Ray tomography. *Acta Materialia* 2005; 53: 719–730.
23. Brydon AD, Bardenhagen SG, Miller EA, et al. Simulation of the densification of real open-cell foam microstructure. *J Mech Phys Solids* 2005; 53: 2638–2660.
24. Daphalapurkar NP, Hanan JC, Phelps NB, et al. Tomography and simulation of microstructure evolution of a closed-cell polymer foam in compression. *Mech Adv Mater Struct* 2008; 15: 594–611.

25. Jeon I, Asahida T, Kang K-J, et al. Finite element simulation of the plastic collapse of closed-cell aluminum foams with X-ray computed tomography. *Mech Mater* 2010; 42: 227–236.
26. Wismans JGF, van Dommelen JAW, Govaert LE, et al. X-ray computed tomography based modeling of polymeric foams. *Mater Sci Forum* 2010; 638–642: 2761–2765.
27. Caty O, Maire E, Youssef S, et al. Modeling the properties of closed-cell cellular materials from tomography images using finite shell element. *J Acta Materialia* 2008; 56: 5524–5534.
28. DIN EN 826. Thermal insulating products for building applications - determination of compression behaviour. Berlin: Beuth, 1996.
29. Herman GT. *Image reconstruction from projections*. New York: Academic Press, 1980.
30. Chen Y, Vemuri BC and Wang L. Image denoising and segmentation via nonlinear diffusion. *Comput Math Appl* 2000; 39: 131–149.
31. Elmoutaouakkail A, Salvo L, Maire E, et al. 2D and 3D characterization of metal foams using X-ray tomography. *J Adv Eng Mater* 2002; 4: 803–807.
32. Brisco BJ, Fiori L and Pelillo E. Nano-indentation of polymeric surfaces. *J Phys D: Appl Phys* 1998; 31: 2395–2405.
33. Zeng K. Nanoindentation and indentation creep of polymeric materials. In: Sinha SK, Briscoe BJ (eds) *Polymer tribology*. London, UK: Imperial College Press, 2009.
34. Fischer-Cripps AC. *Nanoindentation*. New York: Springer, 2004.
35. Pharr GM and Oliver WC. An improved technique for determining hardness and elastic modulus using load and displacement sensing indentation experiments. *J Mater Res* 1992; 7: 1564–1583.
36. Matonis V. Elastic behavior of low density rigid foams in structural applications. *SPEJ* 1964; 20: 1024–1030.
37. Chan R and Nakamura M. Mechanical properties of plastic foams: the dependence of yield stress and modulus on the structural variables of closed-cell and open-cell foams. *J Cell Plast* 1969; 5: 112–118.
38. Nammi SK, Myler P and Edwards G. Finite element analysis of closed-cell aluminum foam under quasi-static loading. *Materials Des* 2010; 31: 712–722.
39. Habbit D, Karlson B and Sorenson P. *User's manual and theory manual*. Providence, RI: Dassault Systèmes, 2010.